Evaluation of an improved AROME configuration for fog forecasts during the SOFOG3D campaign

Salomé Antoine, Rachel Honnert, Yann Seity, Benoît Vié, Frédéric Burnet, Pauline Martinet

Evaluation of an improved AROME configuration for fog forecasts during the SOFOG3D campaign.

Salomé Antoine,[1] , Rachel Honnert,[1] Yann Seity,[1] Benoît Vié,[1] Frédéric Burnet[1] Pauline Martinet [1]

[1] *CNRM, Université de Toulouse, Météo-France, CNRS, Toulouse, France.*

Corresponding author: Salomé Antoine, salome.antoine@meteo.fr

ABSTRACT: This paper evaluates fog forecasts of a new AROME configuration dedicated to fog thanks to observations of the recent field campaign SOuth westFOGs 3Dimensions (SOFOG3D). This new configuration takes advantage of an upgraded horizontal and vertical resolution, of a 2-moment microphysical scheme (LIMA) and of the inclusion of a parametrization of the droplets deposition onto vegetation. A statistical study conducted over the 6 months of the SOFOG3D field campaign allowed the evaluation of the quality of fog forecasts produced by this new configuration to compare it to the current operational configuration of AROME. The main findings are as follows: the new configuration forecast more fog events, with a few more false alarms, but improved the amount of fogs with low top height and with a low water content, underestimated by the reference configuration. The importance of the first level height for a good representation of the first few meters above the ground is crucial to improve the fog formation forecast. A delay of fog dissipation in the morning was highlighted in operational simulations and slightly reduced thanks to LIMA. This two-moment scheme produced thinner fogs, with less water content. These are more realistic, compared with observations, and thinner fog is also easier for solar radiation to dissipate.

1. Introduction

Fog is defined as a suspension of water droplets in the air, which reduces horizontal visibility at the lowest levels of the atmosphere near the surface (World Meteorological Organisation 2017). Issues linked to fog are multiple, both in terms of security wise and economics. As mentioned by Gultepe et al. (2009), the financial impact of fog is similar to that of winter storms. No sector appears to be excluded, whether it is aviation (Mathew et al. 2016; Gultepe et al. 2019), marine shipping (Fernando et al. 2021), road transport (Pagowski et al. 2004), or sports and social activities (Pezzoli et al. 2010). In the aviation sector, fog is a problem for aircraft takeoffs and landings: fog may trigger Low Visibility Procedures, leading to flight delays and economical losses by reducing the frequency of takeoffs and landings or diverting aircraft (Gadher and Baird 2006; Milmo 2007). The main mechanisms involved in fog formation are relatively well known. Based on these elements, a fog event can be classified as proposed by Tardif and Rasmussen (2007). The most frequent fogs over land are radiative fog (Bergot 2013), advection-radiative fog (Ryznar 1977) and stratus lowering fog (SLF) (Dupont et al. 2012). However, these mechanisms have low predictability (Bergot and Koracin 2021). To limit fog-related problems, forecasters and airline companies are interested in improving fog forecasting, both temporally and spatially.

Given their societal and economical importance, fog forecasts are necessary to mitigate its impact on human activity (Gultepe et al. 2009), even in the relatively short term, from a few hours to 2 days. Among the various methods developed and used over the last decades, Numerical Weather Prediction (NWP) models are nowadays the most commonly used systems for short-term fog forecasts (Price et al. 2018). These models, developed by national meteorological offices for operational purposes, are usually limited-area models at the kilometer scale, initialized after assimilation of fine-scale observations. Such NWP models include for instance, Application of Research to Operational at MEso-scale (AROME, Seity et al. (2011); Brousseau et al. (2016)) over France, HARMONIE (HIRLAM ALADIN Research on Mesoscale Operational NWP In Euromed, Bengtsson et al. (2017)) over different European countries, COSMO (COnsortium for Small-scale MOdelling, Bentzien and Friederichs (2012)) over Germany, Swiss and Italy.

Many previous studies with operational NWP have assessed the performances of fog forecasts, by comparing them to regular observation networks, as in Gultepe et al. (2007a) where Canadian

operational NWP model was compared to satellite and surface observations. For instance, Román-Cascón et al. (2019) studied fog forecast by the HARMONIE model in the Spanish Northern Plateau and the proportion of radiative fogs and SLF forecast in this region. The model had more facility in forecasting SLF than it did radiative fogs. The duration and fog top height of this kind of fog were overestimated however and the model had difficulty predicting a situation with alternating radiative and SLF. Even Westerhuis et al. (2020) found that the COSMO model underestimated persistent fogs on the Swiss Plateau and they attempted to reduce this bias. Changing a microphysical scheme from a one-moment to a two-moment scheme or altering the vertical grid did not lead to an improvement, whilst reducing the lower bound for turbulent mixing coefficient or improving the horizontal grid allowed the delay of fog dissipation. Fog forecasts computed by operational AROME were studied by Philip et al. (2016). They evaluated the impact of vertical resolution on fog forecasts with kilometric-scale AROME. This study was achieved as a case study and statistically during an entire winter season over Paris Charles de Gaulle Airport (Paris-CDG), France. They showed a strong impact of vertical resolution on fog onset and thermodynamic proprieties in fog, highlighting the importance of a fine vertical resolution close to the ground in order to forecast fog. These results were consistent with those of Tardif (2007) who studied the impact of vertical resolution on fog forecasts with a one-dimensional model: fog onset processes were impacted by vertical resolution and were more realistic with a finer grid. The importance of near-surface resolution in the quality of fog forecast has been confirmed in the recent model intercomparison Boutle et al. (2022). In addition, Philip et al. (2016) highlighted an underestimation of SLF forecast by the AROME model over Paris-CDG. This report led to the work of Fathalli et al. (2022), where they studied this kind of fog event in the North of France in order to investigate the processes responsible for its formation. More recently, Bell et al. (2021) studied the impact of assimilation of new observations data, from radiometers, on the quality of fog forecasts by the AROME model.

Fog formation and life cycles are driven by fine processes (Gultepe and Milbrandt 2007; Bergot 2013; Price and Clark 2014; Gultepe et al. 2021): turbulent, microphysical, thermodynamic and radiative processes. Some of these processes are hardly observable, and so even harder to forecast, for example when one considers the impact of tree barriers on fog formation and the collection of droplets by vegetation (Mazoyer et al. 2017) or the effect of small-scale surface heterogeneities and buildings (Bergot et al. 2015).

In order to improve the AROME forecasts, a new configuration has been developed, which includes an increase in horizontal and vertical resolution, a new two-moment microphysical scheme, and the taking into account of an important physical process, the droplets deposition on vegetation. Many of these improvements have been tested in research models (such as Meso-NH, Lafore et al. (1998); Lac et al. (2018)) on specific case studies and independently of each other.

A fine horizontal resolution allows a better representation of surface heterogeneities and orography, particularly relevant during the formation phase (Bergot et al. 2015) or for the forecasting of valley fogs (Ducongé et al. 2020). For instance, the United Kingdom Met Office has run a 333 m horizontal resolution NWP model since 2013 around Heathrow airport, the *London Model* (Boutle et al. 2016). *London Model* kept the same vertical resolution as their current mesoscale model, i.e. 70 vertical levels with a model top at 40 km. The turbulent and cloud parametrizations were however improved.

The microphysical scheme used to represent the hydrometeors' life cycle is a key component for fog forecasts in NWP models, and more particularly during dissipation phase (Zhang et al. 2014; Stolaki et al. 2015; Steeneveld and de Bode 2018). A one-moment schemes allow the prognostic forecast of one parameter per microphysical species, commonly the mixing ratio, as in ICE3 (Pinty and Jabouille 1998) AROME's operational microphysical scheme. As droplet concentration, and therefore droplet size, impacts fog sedimentation and radiative budgets, it is worth calculating this prognostically. Moreover, droplet concentration may have a significant impact during thin to deep fog transition (Boutle et al. 2018). Two-moment microphysical schemes enable the prognostic forecast of two parameters per microphysical species, such as mass mixing ratios and their concentration, as in the Liquid Ice Multiple Aerosols (LIMA) microphysical scheme (Vié et al. 2016). Under foggy conditions, LIMA has shown a more accurate representation of cloud droplets (Ducongé et al. 2020). The authors used a high-resolution simulation (100 m) in order to understand the impact of local circulation on fog formation and to evaluate simulations with ICE3 and LIMA. They found that LIMA improves fog forecasts, especially when the prognostic droplet number concentration was used in the radiative scheme to calculate cloud optical properties: the radiative impact of droplet concentration is greater than its gravitational settling effect. The importance of agreement with the use of microphysical properties to calculate optical properties

in the radiative scheme had also been mentioned in the intercomparison proposed by Boutle et al. (2022).

Droplet deposition is defined as the collection of fog droplets by vegetation (trees, grass, etc). This process is crucial in fog as shown by von Glasow and Bott (1999), Price and Clark (2014) or Zhang et al. (2014). There is a need to take into account the fact that the deposition should decrease Liquid Water Content (LWC) and droplet concentration in the first meters above the surface as shown by Mazoyer et al. (2017) in the research NWP model Meso-NH. Thus, cloud water content in fog forecasts is more realistic.

This paper assesses whether recent advances in fog forecast modelling, such as the resolution or microphysical parametrization mentioned above, may improve the quality of AROME NWP fog forecasts.

For this purpose, AROME forecasts will be evaluated against measurements collected during the SOuth westFOGs 3Dimensions (SOFOG3D) experiment for processes study led by Météo-France (Burnet et al. (2020)). This six months field experiment has been conducted from October 2019 to March 2020 in the South-West of France to provide three dimensions mapping of the boundary layer during fog events by combining remote sensing instruments, balloon-borne in-situ measurements and a network of surface stations. This dataset, and in particular the microphysical measurements, allow us to deeply evaluate and understand the different AROME configurations for fog forecasts.

Paper begins in section 2 with a description of the SOFOG3D field campaign and observations used. Section 3 presents the NWP AROME model and configurations used in this study. Section 4 details the path taken to detect fog conditions in observations and in forecasts. Section 5 is dedicated to the statistical evaluation of fog forecasts' quality of a new high-resolution configuration, against SOFOG3D data. Section 6 provides analyses and discussions of the model behavior highlighted earlier before the conclusions of the article.

2. Observations

This section is dedicated to the presentation of the SOFOG3D field campaign and the measurements used in this paper to evaluate model forecasts.

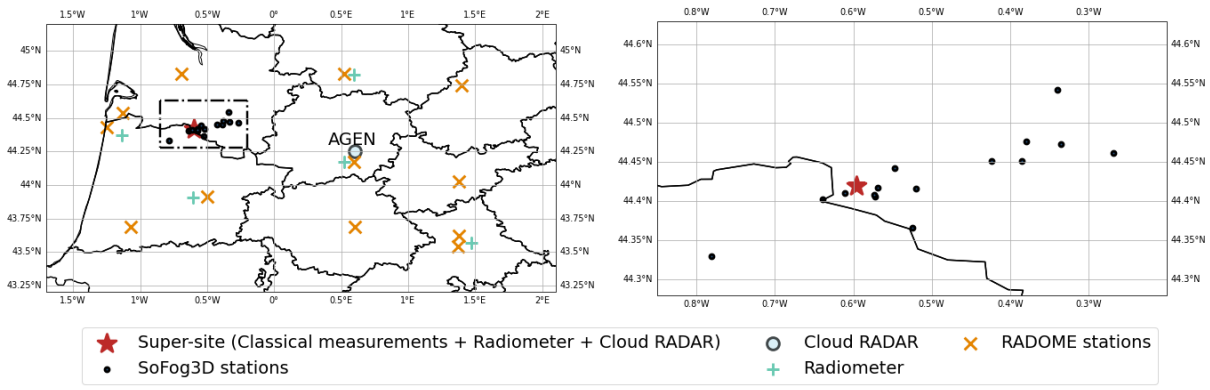

17 FIG. 1. Localisation of the observation sites during the SOFOG3D campaign, across the whole of the southwest
18 of France (on the left) and around the Super site (dashed line on the left and on the right).

The SOFOG3D field observation campaign took place in the southwestern part of France between October 2019 and March 2020. The main site was located near Saint-Symphorien (LAT:44.419548° N ; LON:0.596224° W ; ALT:69m). The location's variety of vegetation types made it possible to assess the impact of surface heterogeneities on fog.

A dense network of sensors consisting of 16 stations was installed around the main site during the field campaign. Their locations are indicated in figure 1. This network was complemented by 12 observation stations of the operational network of Météo-France, the RADOME network (Réseau d'Acquisition de Données et d'Observations Météorologiques Étendu). All these stations allowed continuous monitoring of atmospheric conditions during the campaign. The information provided by in situ facilities included two-meter temperature, two-meter relative humidity, ten-meter wind speed and three-meter horizontal visibility. The available observations used in this study are summarised in the table 1.

In addition, two cloud radars (Delanoë et al. 2016) and six radiometers (Martinet et al. 2022) were installed throughout the southwest of France. The deployed cloud radars were Bistatic Radar System for Atmospheric Studies (BASTA) cloud radars with a 95-GHz frequency-modulated continuous wave Doppler radar covering the atmosphere from 50 m height to 10 km height. They allowed the estimation of fog top height, if it was higher than 50 m. Liquid Water Path (LWP) and temperature profiles were obtained using radiometer measurements. On the Jachère site, located near Super-site, a FogMonitor (FM-120, Droplet Measurement Technologies Inn., Boulder, CO,

TABLE 1. Characteristics of main sensors installed during SOFOG3D field campaign and used in this study.

Measurement	Instrument	Number	Height	Uncertainty
Visibility	PWD 22/52 of Vaisala 73000 Sentry of Young	6 13	3m	10%
RADOME Visibility	PWD 22/52 of Vaisala	11	3m	10%
LWC Droplet concentration	CDP	1	tethered balloon	
LWC Droplet concentration	FM-120	1	3m	+/- 10%
LWP	Microwave radiometer	6	remote sensing	+/- 20 g.m^{-2}
Fog depth	95 GHz cloud radar BASTA	2	remote sensing	from 50 m

U.S.A., Gultepe et al. (2007b); Spiegel et al. (2012)) was installed to measure the distribution of droplets in the clouds, allowing the determination of droplet concentration and LWC.

When the weather situation was favorable for the development of fog at the Super-site, additional observation systems were deployed during Intensive Observation Periods (IOP). During the six months of SOFOG3D campaign, there were 15 IOPs with 20 nights of observations. During IOPs, complementary observations included (1) radiosoundings and (2) a tethered balloon measurements equipped with a turbulent probe (Canut et al. 2016) and a Cloud Droplet Probe (CDP). The CDP measures the size distribution of water droplets within a diameter range from 2 to 50 μm, that allows to follow the evolution of LWC and droplet concentration at various altitude level in the fog layer Fathalli et al. (2022).

3. NWP model description

This section is dedicated to the description of the forecast system used in the study.

In this study, simulations were performed with the French non-hydrostatic limited-area model Application of Research to Operational at MEso-scale (AROME, Seity et al. (2011); Brousseau et al. (2016)). AROME was developed in order to forecast high impact meso-scale meteorological phenomena, such as fog, thunderstorms or heavy rains. Over France, it has been used operationally in Météo-France since December 2008.

In this study, a forecast domain was implemented over an area of 200x300 km centered in the southwest of France, shown in figure 2. Runs were performed between October 2019 and March 2020 with forecasts starting at 0000 UTC and lasting 48h. These simulations were initialized by AROME-France operational analyses and were coupled hourly with AROME-France operational forecasts. The main characteristics of the reference simulation are detailed in table 2. This configuration, referred to as 1250L90 in the following text, was similar to the operational AROME-France configuration, except when concerning the closure mass flux coefficient.

The intensity of the mass-flux at the surface (Pergaud et al. 2009) was controlled by a mass-flux closure coefficient set to 0.03 as recommended by Grant (2001) to fog forecast, versus 0.065 in the operational version of AROME-France, in order to reduce the mixing. The mass-flux parametrization represents convective boundary layer thermals which appear at sunrise and increase turbulent mixing: indeed decreasing this coefficient should play a role in fog dissipation. As explained in Pergaud et al. (2009), the operational value was specifically set to improve the forecast of shallow cumulus over a continental area. In their study, Philip et al. (2016) highlighted a model tendency to dissipate fog too early. Complementary work done in Philip (2016) showed better results with the mass-closure coefficient recommended by Grant (2001). In this study, we decided to follow the recommendation made by Philip (2016) and Grant (2001) and set the coefficient to 0.03.

Hectometric simulations evaluated in this study were based on the AROME-France configuration, with some new features detailed in table 2. Horizontal resolution was refined from 1250 m to 500 m. Vertical resolution was significantly improved, from 90 vertical levels (with a first level at 5 m) in AROME-France to 156 vertical levels (with a first level at 1 m). The new vertical grid is the same as the finest vertical grid in Philip et al. (2016), which provided the best results for fog forecasts. This new configuration will be referred to as 500L156 in the following.

The microphysical scheme used in 1250L90 was the one-moment scheme ICE3 (Pinty and Jabouille 1998), in which only the mass mixing ratio [$kg.kg^{-1}$] is prognostic for cloud droplets. The droplet concentration is always equal to 300 cm^{-3} over land and 100 cm^{-3} over sea. The 500L156 simulation used LIMA (Vié et al. 2016), a two-moment microphysical scheme in which cloud droplets are described by two prognostic variables: mass mixing ratio and droplet concentration.

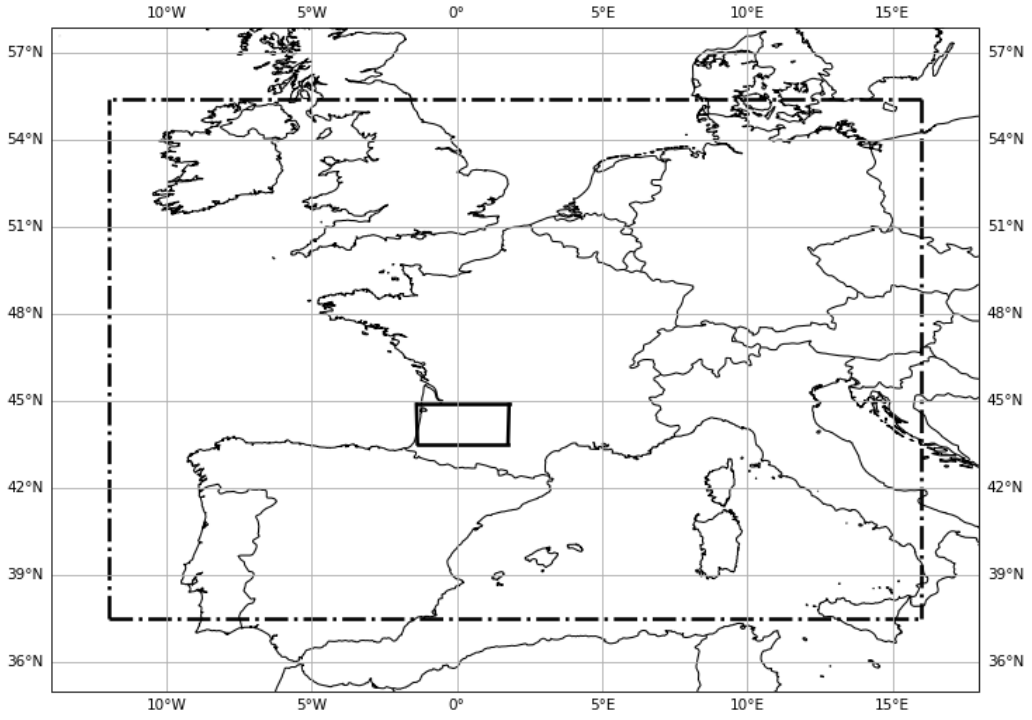

FIG. 2. AROME-France forecast domain (dash line -··-) and domain used in this study (solid line -).

The cloud optical proprieties (effective radius for example) used in the radiative scheme were computed consistent with microphysical prognostics variables. In the reference simulation, using ICE3 microphysical scheme and an droplet concentration over land fixed at 300 cm^{-3}, the optical proprieties of the warm clouds were computed according to the Martin et al. (1994) parametrization and depending only on the LWC. In simulation using the LIMA microphysical scheme, the both prognostics LWC and N_c were used to compute warm cloud optical proprieties.

LIMA allows several free Cloud Condensation Nucleus (CCN) initializations: (1) an empirical constant starting value, (2) information from a real time aerosol/chemistry NWP model or (3) observations. In this study, a constant value of 300 cm^{-3} was provided as the initial number of free CCN, with a size distribution centered around the mean radius of 0.12 μm and $log(\sigma) = 0.69$. Droplet concentration was obtained from free CCN by activation processes explained in section 2.2 of Vié et al. (2016), pages 570-571.

In both model configurations, the operational subgrid condensation scheme implemented in AROME-France was used. This scheme depends on the parameters computed by the turbulence

TABLE 2. Main characteristics of the reference simulation (1250L90) and the hectometric simulation (500L156).

Configuration	1250L90 - Reference	500L156 - Hectometric
Lateral boundary conditions	AROME-France forecasts	
Horizontal resolution	1250m	500m
Number of vertical level	90	156
First level height	5m	1m
Number of level bellow 500m	15	53
Starting time	0000UTC	
Simulation duration	48h	
Outputs frequency	1h	
Closure mass-flux coefficient	0.03 (Grant 2001)	
Sub Grid condensation	Yes	
Microphysical scheme	ICE3	LIMA
Droplet deposition	No	Yes
Droplet concentration	300 cm^{-3} over land 100 cm^{-3} over sea	prognostic variable
Free CCN initialisation	-	Constant value - 300 cm^{-3} ($\overline{r}$=0.12 μm ; $log(\sigma)$=0.69)
Cloud optical properties	Martin et al. (1994)	Based on prognostic LWC and N_c

scheme (subgrid variance of the departure to saturation, very low in stable case and in fact in foggy situations) and by a climatological variance (Rooy et al. 2010; de Rooy et al. 2022). The climatology variance proposed by Rooy et al. (2010) is associated to a critical relative humidity of 96 %.

As explained in Zhang et al. (2014), the deposition of fog droplets on vegetation is an important process for fog evolution. Different methods are possible to parameterize the deposition of droplets on vegetation. The formulation can be more or less complex depending on the prognostic variables available and used. In Gultepe and Milbrandt (2007), the authors proposed a formulation that depends on LWC and droplet concentration (N_c), while Zhang et al. (2014) or Mazoyer et al. (2017) proposed formulation that depends only on LWC. In our study, we used a formulation that can be applied in both in the ICE3 and in the LIMA microphysical scheme. The deposition flux

($F_{deposition}$ [$kg.m^{-2}.s^{-1}$]) follows a simple relationship between the deposition velocity ($V_{deposition}$ [$m.s^{-1}$]) and the LWC [$kg.m^{-3}$] in the lowest level of the atmospheric model, as shown in Eq.1.

$$F_{\text{deposition}} = V_{\text{deposition}}.\text{LWC}. \tag{1}$$

Deposition flux was only active when cloud water was present at the lowest level and reinforces the loss of cloud water by sedimentation already present between this level and the surface. As the droplets fall from the upper levels by sedimentation, the deposition impacts several levels above the surface. As shown in Katata (2014) or Mazoyer et al. (2017), deposition rate is delicate to set and is highly uncertain. As deposition parameterization is newly introduced in AROME model, we decided to start with a simple approach and a constant $V_{deposition}$ of 2 $cm.s^{-1}$ whatever the vegetation, as in the reference simulation in Mazoyer et al. (2017). Currently, deposition is not taken into account in operational AROME-France configuration, thus deposition is not taken into account in our reference configuration.

4. Detection of fog conditions

During the SOFOG3D field campaign, 18 visibility sensors were installed at 16 different sites in order to identify fog situations. In addition, every RADOME stations were fitted with a visibility sensor. Therefore, we took advantage of this network and we defined the observed fog events with a threshold of 1000 m on the visibility observed by field measurements (see more details in Tab. 1). Different tests were performed to check the impact of taking into account precipitation in the detection of fog episodes (not shown). As the results were not significantly different, only the threshold on the visibility parameter was kept. Visibility parameter was available several times per hour in almost every station of the forecast domain. So, in order to compare observations and forecasts, the observed visibilities were reprocessed to use the minimum visibility of the past hour. Thus, a fog event occurred when the minimum visibility in the past hour was less than 1000 m.

In the NWP model, visibility is not a prognostic variable and need to be diagnosed. As the wide range of available visibility parameterizations shows (Long et al. 2021), diagnosing visibility is a complex task. In addition, visibility formulation is often established from observations (Kunkel 1984; Gultepe et al. 2006) and depends on this database. Diagnoses can be adapted to the forecasts

of each NWP model, as was done in Philip (2016). Nevertheless, the study presented in this paper considered multiple model configurations and a single fit of the visibility formulation would be advantageous for one of the model configurations. On the contrary, a formulation adapted to each model configuration would amount to not having the same variable in order to compare simulations. For this reason, we chose not to diagnose visibility for the detection of fog in model forecasts, and to remain closer to model prognostic fields. In the NWP, we therefore decided to detect fog by using the maximum of LWC in the past hour, computed at 5 m height. A LWC threshold, noted Q_{LWC}, was used to distinguish fog and non-fog conditions based on SOFOG3D measurements. The method used to determine this threshold is explained in the rest of this section. Determining Q_{LWC} from SOFOG3D measurements allowed a threshold totally independent from the NWP model.

To determine Q_{LWC}, visibility and microphysical measurements made at the Jachère site were used, when continuous measurements during the six month period were performed by a PWD and a FM-120 sensors, respectively. Microphysical measurements made by FM-120 needed however to be processed in order to remove instrumental noise and in order to be compared with visibility observations. The sampling frequency of FM-120 measurements (1 s) was greater than the frequency of independent visibility measurements (1 min). FM-120 LWC observations were then averaged over a 1 min windows before being compared to visibility. The FM-120 data analysis showed that a large part of droplet concentration and LWC values correspond to high visibility values provided by the PWD, which has no physical reality. Thus a filter was applied to the observations to remove these unrealistic data. As Q_{LWC} is a threshold for LWC, a filter was applied on the droplet concentration measurements so as not to interfere with the LWC values. Different thresholds were tested: 0.01, 0.1, 1 and 2 cm^{-3}, but a too low value did not allow to remove the non physical measurements. Only FM-120 measurements associated with a droplet concentration therefore greater than 2 cm^{-3} were retained.

To compute $\mathrm{Q_{LWC}}$, the logarithms of LWC and visibility were compared and a linear regression was performed in order to establish a relationship between them. The results are shown on figure 3a. From linear regression, a 1000 m visibility was associated to a $\mathrm{Q_{LWC}}$=0.00475 $\mathrm{g.m}^{-3}$. ROC curve (Receiver Operating Characteristic curve) (Fig. 3b) allowed to locate this value among other LWC

thresholds. The LWC value which minimizes false alarm rates and minimizes detection rates was 0.0108 g.m^{-3}. Q_{LWC} was higher than this value, but it allowed to improve the detection rate without increasing the number of false alarms too much. Kunkel (1984) suggested a threshold of 0.018 g.m^{-3} to distinguish fog and non-fog conditions. But using this value would lead to a significant and unrealistic decrease of detection rates in our case (Fig. 3b). Furthermore, the statistical study was realized with different threshold values and the conclusions remained unchanged. Thus, we decided to keep the threshold obtained with the SOFOG3D observations, Q_{LWC}=0.00475 g.m^{-3}.

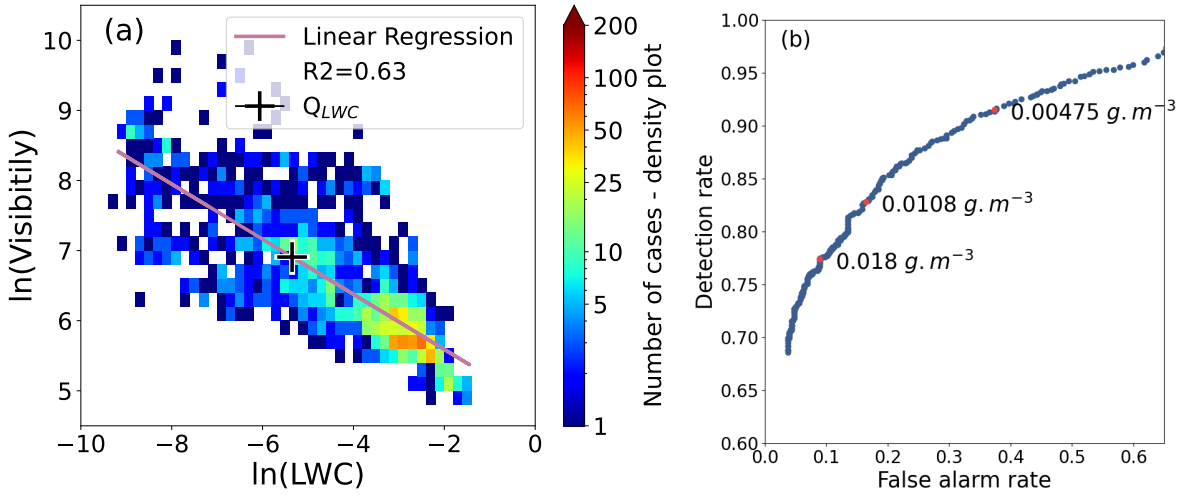

FIG. 3. (a) Scatter plot and linear regression between ln(LWC) and ln(Visibility) observed at the Jachère site during SOFOG3D field campaign. (b) ROC curve according to different LWC thresholds used to distinguish fog and non-fog conditions at the Jachère observation site.

5. Results of the statistical evaluation

This section begins with the presentation of the methodology used to compare the models to the observations. An evaluation of fog forecasts quality with the computation of different statistical scores is then given. Finally, the fog life cycle is examined, as well as fog structure.

a. Observations/forecasts comparison framework

The simulations evaluated in this study started at 0000 UTC (0100 LOC), with a duration of 48 h. In order to evaluate the forecasts over an entire night, the forecasts between the lead time

TABLE 3. Fog forecast quality evaluated on all available measurement stations (between 11 and 18) by HR, FAR and FBI scores. A bold score means that 500L156 score is significantly different from the 1250L90 score (Bootstrap method at 5% level).

Forecast lead time	Simulation	HR (%)	FAR (%)	FBI
+18 to +24	1250L90	48	44	0.86
	500L156	**62**	**56**	**1.41**
+25 to +30	1250L90	60	40	1.0
	500L156	**71**	47	**1.35**
+31 to +36	1250L90	50	59	1.43
	500L156	60	65	**1.71**
+18 to +36	1250L90	63	35	0.96
	500L156	**74**	**44**	**1.32**

+18 (1800 UTC or 1900 LOC day D) and the lead time +36 (1200 UTC or 1300 LOC day D+1) were studied. In order to obtain an accurate representation of the fog life cycle, each night was divided into 3 periods: (1) from lead time +18 (1800 UTC day D) to +24 (0000 UTC day D+1) corresponding to the beginning of the night, (2) from lead time +25 (0100 UTC day D+1) to +30 (0600 UTC day D+1) corresponding to the middle of the night and (3) from lead time +31 (0700 UTC day D+1) to lead time +36 (1200 UTC day D+1) corresponding to the end of the night and the morning. For each of these periods, different scores were calculated to evaluate the quality of the fog forecasts. The life cycle dynamics, structure and microphysical properties of the fogs were then studied over the entire night. Each fog events were detected according to the method explained in the last section (Sec. 4). In addition, each measurement site was compared to the closest model point.

b. Fog forecast quality scores

The quality of fog forecasts was evaluated according to three scores: (1) Hit Rate (HR) and (2) False Alarm Rate (FAR), which evaluate respectively the percentage of fog events detected and the percentage of fog false alarms and (3) Frequency Bias Index (FBI), which provide information about over/under-estimation tendencies of the model. The more FBI was close to 1, the more the number of fog events forecast by the model was close to the number of observed fog events over

the same period. In continuity, it is necessary to have the highest possible HR while keeping a FAR low. The formulation of each score is provided in Appendix A.

First of all, the total number of number of fog hours for selected measurement sites can be compared. At the Agen site, 542 hours of fog were observed during the SOFOG3D field campaign. Over the same period, 1250L90 simulated 518 hours of fog and 500L156 638 hours. At the Jachère site, 267 hours of fog were observed versus 509 and 670 hours simulated by 1250L90 and 500L156 respectively.

Then, the scores were computed over the entire SOFOG3D period, at all available measurement sites within the model's forecast domain (Fig. 1). The fog forecast quality scores for the reference simulation, 1250L90, and the new model configuration, 500L156, are given in table 3. A score in bold means that the score of 500L156 is significantly different from the score of 1250L90 score using the Bootstrap method at 5% level.

The FBI increase indicates that 500L156 forecasts more fog events than 1250L90. The difference is statistically significant whatever the period of the night considered. Over the entire night, this difference is still statistically significant. Thus, 500L156 overestimates the number of fog events. These results are consistent with the difference in total forecast fog hours mentioned previously.

An increase in the number of fog events forecast by 500L156 can be seen in HR and FAR. At the beginning of the night and during the middle of the night, the HR was significantly improved with 500L156, but associated with an increase of the FAR. During the rest of the night, the differences were not significant. Overall, over the entire night, HR and FAR were significantly increased with 500L156, with a slightly larger improvement of HR than degradation of FAR.

c. Fog life cycle dynamic

To complete score computations and to better understand differences between the different parts of the night, the fog life cycle dynamics during the night was studied, at all available measurement sites inside the model's forecast domain during SOFOG3D duration (Fig. 1):

- The fog onset is the first lead time of the night, between +18 (1800 UTC day D) and +36 (1200 UTC day D+1), when a fog event is detected. If the fog event had already started at 1800 UTC day D, fog formation time was set at 1800 UTC.

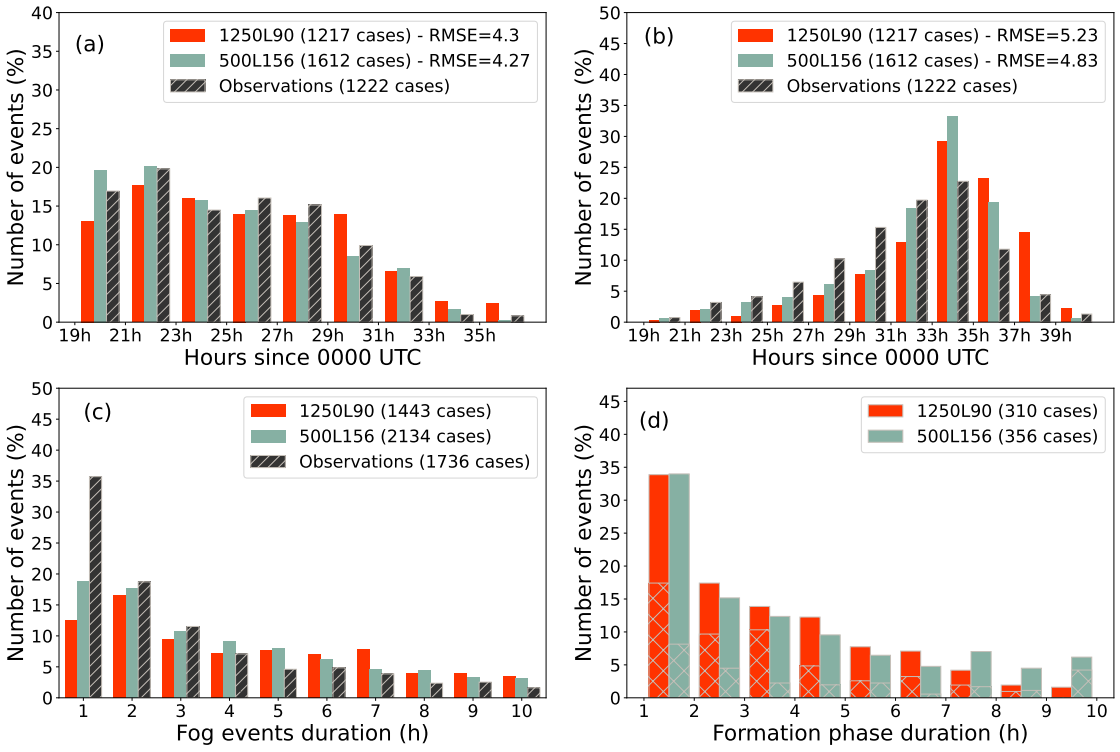

FIG. 4. (a) Distribution of fog formation time, (b) distribution of fog dissipation time, (c) distribution of fog event duration and (d) distribution of fog formation phase duration, the hatch part represents the proportion of formation phases followed by mature phases. Distributions were computed for each fog night occurring between the 14th October 2019 and the 31th March 2020 at all measurement sites. Comparison was made between observations (black hatched bars) and 1250L90 (red bars) and 500L156 (green bars) forecasts. The number in brackets is the number of values taken into account in order to calculate the percentage. RMSE was computed when a fog event was forecast and observed during the night.

- The fog dissipation hour is the last lead time of the night, between +18 (1800 UTC day D) and +36 (1200 UTC day D+1), when a fog event is detected. If fog was not dissipated at 1200 UTC, the real dissipation hour was looked for, until the end of the simulation.
- The fog event duration is the number of consecutive hours during which a fog event was detected. One night could be concerned by more than one fog event.
- The duration of the fog formation phase is the number of hours before the fog becomes mature or dissipates. The beginning of the mature phase is defined as the first hour when LWC is higher than Q_{LWC}, the net surface Long Wave (LW) is close to zero (+/- 5 W.m^{-2})

and the temperature difference between the first model level and 50 m is close to zero (+/- 0.01 $K.m^{-1}$) (Bergot and Lestringant 2019). This definition is only valid for radiative fog. This parameter is computed only for radiative fog therefore according to the fog classification algorithm of Tardif and Rasmussen (2007). However, the available observations did not allow the calculation of this parameter in the observations

The distribution of fog formation onset for both simulations is compared to observations on figure 4a. The number of fog events which began before lead time +23 was underestimated in 1250L90 forecasts. Underestimation was reduced in 500L156 forecasts.

This result is consistent with scores computed in table 3: the number of fog event forecast at the beginning of the night by 1250L90 was underestimated with an FBI of 0.86. In the middle of the night, this underestimation was reduced with an FBI of 1.0. In comparison, the FBI of 500L156 at the beginning of the night and in the middle of the night were reduced from 1.41 to 1.35.

Fog dissipation distribution is shown in figure 4b. Both simulations presented a delay in the dissipation of fog compared to observations. The delay was reduced however with the 500L156 simulation. The dissipation delay corresponds to large FBI computed for both simulations at the end of the night, 1.43 and 1.71, respectively (Tab. 3). 1250L90 then underestimated the short fog events compared to observations, this underestimation being a little reduced with 500L156 (Fig. 4c). In addition, overestimation of fog event with a longer lifespan, more than 4 hours, is consistent with a delay in model dissipation.

Figure 4d presents the distribution of fog formation phase duration. Both distributions are relatively close. Nevertheless, 1250L90 forecast a few more events with a short fog formation phase, less than 3 hours. Among these short events, it may be noticed that a large part of them never reached a mature phase among 500L156 fog events compared to 1250L90 fogs. In this way, 500L156 forecast more fog events with a long formation phase, more than 7 hours, compared to the 1250L90 forecast.

d. Structure and microphysical properties of fogs

In order to further investigate fog forecasts, we will now focus on in-cloud parameters, such as fog depth and microphysical characteristics. Thus, the predicted fog structures were studied and compared to observations when possible.

Firstly, the fog top height is determined. In the simulation, fog top height is the maximum altitude at which the LWC is higher than Q_{LWC}, continuously from the ground. In the observations, fog top height was determined with cloud radar reflectivity, when observed ground visibility was below 1000 m. However, only fogs thicker than 50 m could be observed by the cloud radar. If observed ground visibility was below 1000 m but no signal was observed on cloud radar, an arbitrary depth of 25 m was attributed to fog. The cloud radars were installed on Super-site and Agen site. Only forecasts associated with these two sites were considered.

Fog events studied here were mainly thinner than 300 m. Fogs with higher top height were uncommon: 1, 10 and 27 events in the observations, 1250L90 and 500L156, respectively. Moreover, in the model forecasts, they were often capped by precipitating stratus or stratocumulus.

Figure 5a shows the distributions of the mean fog top height. 1250L90 simulation underestimated thin fogs (less than 50 m) and overestimated thick fogs (more than 100 m). This issue is solved in the 500L156 forecasts, which exhibit a distribution very close to the observations, even if the total number of fog events is overestimated. This result is to be linked with the improvement in the forecast of short fog events with the 500L156 configuration: thin fogs must have a shorter lifespan.

Next, for all fog events detected on the studied night (between 1800 UTC day D and 1200 UTC day D+1), the mean LWP was computed. Figure 5b gives the distribution of mean LWP in the fogs observed by the 6 radiometers (Fig. 1), compared to the mean LWP in the fogs forecast by 1250L90 and 500L156 on the same sites. Firstly, 1250L90 tends to overestimate this quantity. A large proportion of events has a LWP above 30 g.m^{-2} in the 1250L90 forecasts, (Fig. 5b). In comparison, observed LWP were lower than 30 g.m^{-2}. Underestimation was reduced in 500L156 forecasts, with more events with low LWP. Nevertheless, 500L156 continues to overestimate fogs with high LWP (more than 50 g.m^{-2}). This results are consistent with previous observations regarding the fog top height. In thin fog, LWP is generally low. Thus, underestimation of thin fogs results in underestimation of fogs with low LWP, and vice versa for thick fogs.

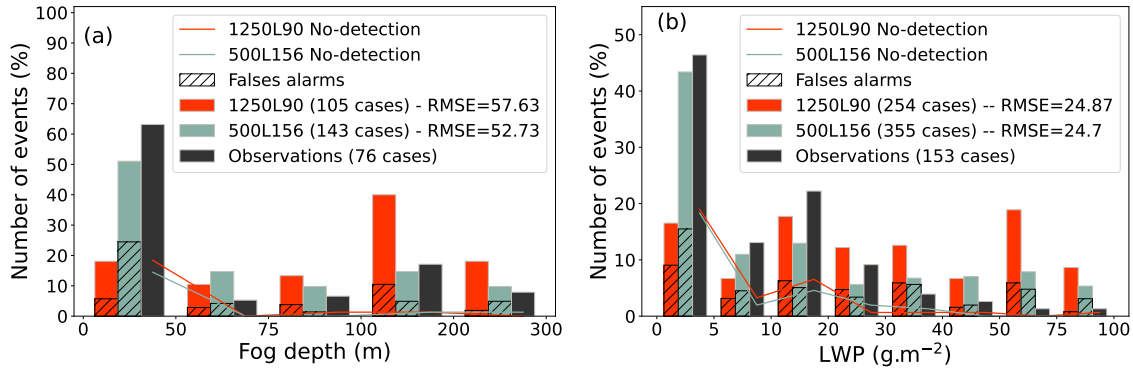

FIG. 5. (a) Mean fog top height distribution computed on Super-site and Agen site forecast by 1250L90 (red bars) and 500L156 (green bars) and estimated from the cloud radar observations (black bars). (b) Distribution of mean LWP observed with radiometers (black bars) and forecast by 1250L90 (red bars) and 500L156 (green bars), computed on the 6 sites equipped with a radiometer. The number in brackets is the number of values taken into account so as to calculate the percentage. RMSE was computed when fog event was forecast and observed during the night. No-detections (resp. false alarms) indicate proportion of undetected (resp. false alarm) events among observations (resp. forecasts) for each model configuration.

A complementary study was performed between fog top height and LWP associated with false alarms and no-detected fog events (Fig.5). In the 1250L90 forecasts, false alarms mainly involved thin and thick fogs (fog top height less than 50 m or more than 100 m), but with weak LWP (less than 20 g.m^{-2}). In the 500L156 forecasts, false alarms were mainly thin fogs with a weak LWP. In both simulations, undetected events were mostly thin fogs with a low LWP.

Finally, droplet concentrations (N_c) forecast in fog were then compared to the tethered balloon observations (Fig. 6a). The observational distribution was computed on measurement data associated at the same time with an observed ground visibility below 1000 m. Observed data were available only during IOP nights, in the Super-site, but every 10 seconds. The forecast distributions were realised with the same method as for fog depth in order to keep data on the whole fog profiles. As comparison between model distributions computed only on IOPs and on over the entire campaign period yielded equivalent results (not shown), distributions computed over the entire SOFOG3D period were kept in figure 6. Only the forecasts at the Super-site are nevertheless kept.

In the 1250L90 simulation, N_c was a fixed value of 300 cm^{-3} over land. However, figure 6 shows that in the observed fogs, droplet concentration was more often lower than 100 cm^{-3}. These values are consistent with previous studies on droplet number concentration in radiative fogs: Mazoyer et al. (2022) although this study was for a suburban area or Gultepe and Isaac (2004) who had found a droplet concentration of 100 cm^{-3} and 200 cm^{-3} for maritime and continental clouds respectively. In stratus lowering fog, droplet number concentration can be more important with values higher than 200 cm^{-3} (Fathalli et al. 2022). In 500L156, N_c was a prognostic variable and forecast values were really more realistic, if a bit underestimated considering the free CCN value chosen here (homogeneous field of 300 cm^{-3}, Tab. 2). This result can be link to the high number of radiative fogs remaining in formation phase in 500L156 forecasts (Fig. 4d). As shown by Boutle et al. (2018), reducing droplet number concentration allows to extend the duration of the development phase in the model.

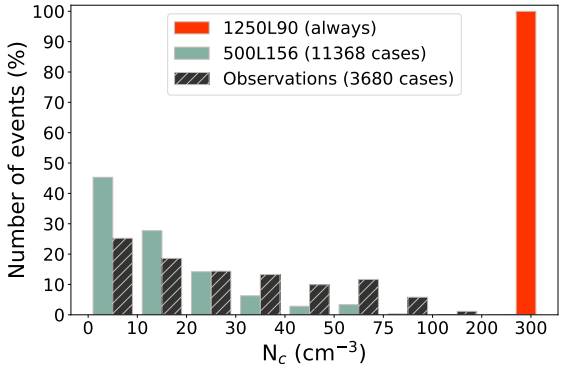

39 FIG. 6. Distribution of N_c observed with CDP (black hatched bars) and forecast by 1250L90 (red bars) and
40 500L156 (green bars) on Super-site.

In this section, fog forecasts of the 500L156 AROME configuration have been evaluated and validated. The statistical study showed an improvement of these forecasts over the quality of the 1250L90 fog forecasts: a more realistic microphysical structure and composition and a reduction of some biases.

6. Analysis and discussion

In this study, the operational configuration of AROME-France was upgraded to a new configuration dedicated to fog forecast. In the previous part, multiple differences and improvements have been noticed in fog forecast quality. This section proposes to provide an explanation for each of the observed differences.

a. Number of fog events

In the first place, more fog events were forecast by 500L156 simulation than with 1250L90 simulation (Tab. 3). A comparison was realised with different vertical grids and a horizontal resolution of 500 m (not shown). The statistical comparison showed that the more vertical levels and the lower the first level near the ground, the higher the number of expected fog events. These results were consistent with the Philip et al. (2016) study done in AROME model. In addition, Tardif (2007) shown that finer vertical grids close to the ground in the model improve the representation of night-time radiative cooling, which is particularly important in the formation of radiative fog. Thus, the increase in the number of fog events predicted by the new model configuration was related to the use of a finer vertical grid. The deposition consideration and the microphysical scheme modification had a smaller impact.

Moreover, the condensation scheme was the same in both configurations. Operational subgrid condensation scheme implemented in AROME-France was used. The scheme depends on parameters computed by the turbulence scheme and a climatological variance proposed by Rooy et al. (2010), associated with a critical humidity of 96 %. In fog situation, it is mostly the second term that is significant. This term is suitable for the 1250L90 configuration, but may be too low for the 500L156 configuration. Condensation is easier the smaller the volume of the layer in the model. Thus, the value might be adapted to the 500L156 grid, as it is in the *London Model* (Boutle et al. 2016). They changed from a critical relative humidity of 96 % at the surface in the kilometric model (1.5 km horizontal resolution) to a critical relative humidity of 97 % at the surface in the hectometric model (333 m horizontal resolution).

b. Formation delay

Figure 4 shows a reduction of formation delay in the 500L156 simulation.

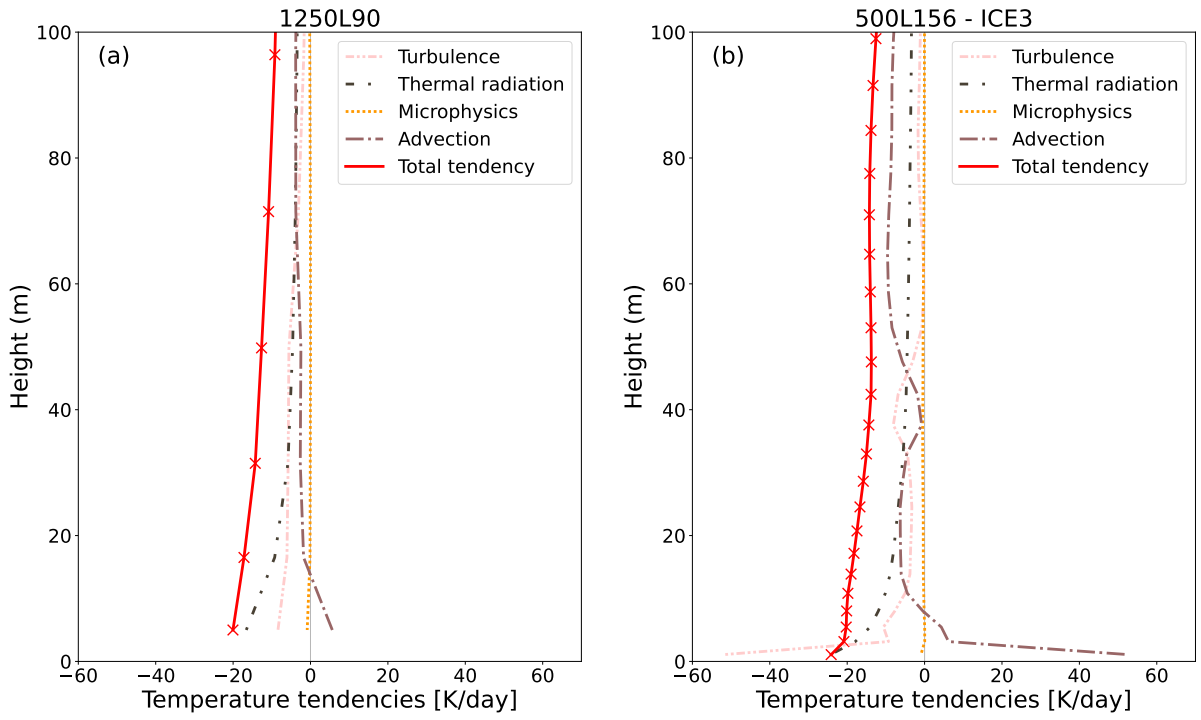

41 FIG. 7. Mean impact of the processes involved in the temperature evolution during the hour of fog formation,
42 fog formation calculated on the formation subset in Agen, (a) for 1250L90 and (b) for 500L156-ICE3. The
43 crosses mark the vertical level of the model.

A first comparison between simulations with ICE3 or LIMA microphysical scheme with the same model grid, allowed to put aside these two modifications (not shown). The same conclusion was found for simulations with and without the droplet deposition process. These differences between 1250L90 and 500L156 could not explain the reduction of formation delay.

To investigate formation delay issues, and to remove the impact of microphysical modifications (although not significant), 1250L90 forecasts were compared to simulations with the same grid as 500L156, but with the ICE3 microphysical scheme and without deposition, referred to as 500L156-ICE3. A subset was then created on the Agen measurement site. A date was conserved if, in 1250L90 forecasts: (1) fog was observed and began between 1800 UTC day D and 0000 UTC day D+1 and (2) fog was forecast and began less than 6h after the observed fog. Subset includes, with this conditions, 22 fog events. Only Agen site was considered here because it was the site

with the highest number of fog hours during the SOFOG3D field campaign and provided the most representative subset.

For all fog events in the subset, 500L156-ICE3 simulation had forecast fog for the night and the delay was reduced compared to the 1250L90 forecasts. According to the algorithm of Tardif and Rasmussen (2007), the fogs in the subset were mainly radiative fogs. During the formation phase of radiative fogs, radiative cooling was propagated vertically by turbulence. Figure 7 shows processes involved in the temperature profile during the hour of fog formation, computed on formation subsets for 1250L90 and 500L156-ICE3 configurations. As the situation considered here was fog formation, no normalization on fog top height has been performed. In both cases, air cooling was associated with thermal radiation and turbulence. Above 20 m, profiles were very similar between the two simulations. Nevertheless, below 20 m, turbulence impact on the lower levels was much greater with the 500L156-ICE3 grid, even if this was partly offset by the advection term. However, air mass mixing was more efficient in 500L156-ICE3 simulations and cooling was propagated faster.

In this way, the difference concerning fog formation was explained by the vertical grid and level density in the first few meters above ground. This result confirms the studies of Philip et al. (2016) and Tardif (2007) which had shown that a high vertical resolution forecast earlier fog formation than a low vertical resolution and the radiative cooling was more realistic with a finer vertical grid, respectively.

c. Fog top height and LWC in fog

500L156 forecast more fogs than 1250L90. Nevertheless, these additive fog events were thinner and with lower water contents (Fig. 5). To understand differences between 500L156 and 1250L90, fog top height and LWP in fog forecast by four model configurations were compared:

- 500L156, the new model configuration evaluated in the previous section, using LIMA microphysical scheme and taking into account of deposition parametrization,

- 500L156-ICE3, a model configuration using the same vertical and horizontal grids as 500L156, but with the microphysical scheme of 1250L90 (ie. ICE3 without taking into account of deposition parametrization and with a droplet concentration set to 300 cm^{-3}),

- 500L156-WOD, the same model configuration than 500L156 but without taking into account of deposition parametrization, and,

- 500L156-NC50, a model configuration using the same vertical and horizontal grids than 500L156, but using ICE3 microphysical scheme, with taking into account of deposition parametrization and with a droplet concentration fixed at 50 cm^{-3}.

Results are shown on Figure 8,computed on the two sites equipped with cloud radars and on the six sites equipped with radiometers respectively. On the one hand, 500L156 significantly improved the distributions of fog top height and LWP in fog compared to 500L156-ICE3. Simulation 500L156 forecast more thin fogs, with a top height below 50 m, and reduced the overestimation of thick fogs, with a top height above 100 m. In addition, 500L156 reduced the overestimation of LWP in fog compared to 500L156-ICE3. In particular, 500L156 allowed the increase of the proportion of predicted fog events with low LWP, less than 5 $g.m^{-2}$. There were no significant differences between forecast with and without taking into account of deposition term however. On the other hand, results obtained with 500L156-NC50 simulation were very similar to those obtained with 500L156, particularly fog thin fog (less than 50 m). Differences between simulations 500L156 and 500L156-ICE3, and more usually 1250L90, should be attributed to droplet concentrations values, prognostic in 500L156 with values lower than the fixed value of 300 cm^{-3} used in 500L156-ICE3 and 1250L90 (Fig. 6). This result was consistent with Boutle et al. (2018), who used a lower cloud droplet number, more representative of fog conditions, to obtain improved fog forecasts.

The same comparison was made with 1250L90 grid and the same conclusions were made (not shown). Thus, the improvement of fog depth and LWP forecasts should be attributed to microphysical scheme modification and especially to the lowed droplet concentration forecast with LIMA compared to set operational ICE3 value, more than to the use of deposition term or grid modifications.

Nevertheless, 500L156-NC50 should not be an operational solution to improved fog forecasts. Indeed, a droplet concentration of 50 cm^{-3} was suitable for the southwest area in fog conditions, but an operational NWP model must adapt to another area and above all to all weather conditions (where droplet concentration were more often higher than 50 cm^{-3}). The use of a two-moment microphysical scheme allows adaptation to all weather conditions.

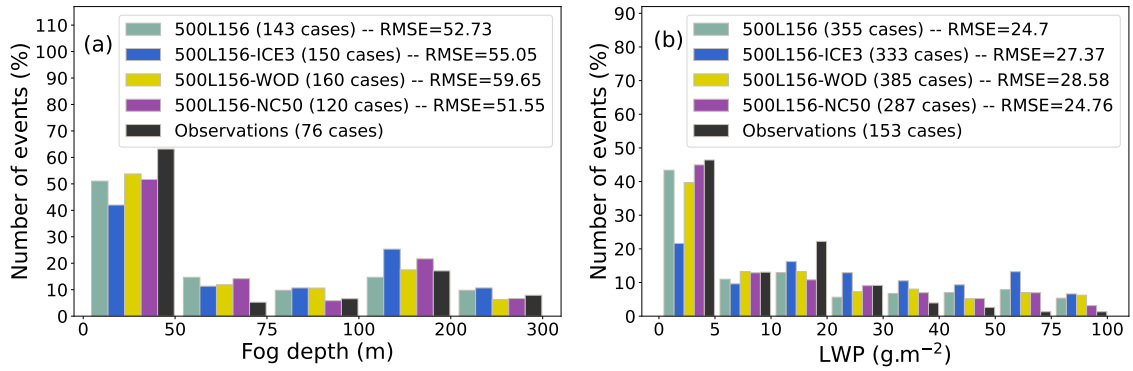

FIG. 8. (a) Distribution of the mean fog top height, computed on the two sites equipped with a cloud radars and (b) mean LWP distribution computed on the 6 radiometer sites; observed (black bars) and forecast by 500L156 (green bars), by 500L156-ICE3 (blue bars), by 500L156-WOD (yellow bars) and by 500L156-NC50 (purple bars). RMSE was computed when fog event was forecast and observed during the night.

Concerning deposition parametrization, there were no significant differences in LWP and fog top height with 500L156 grid and LIMA microphysical scheme (Fig. 8). The main significant difference between simulations with and without deposition parametrization concerns the reduction in LWP overestimation on the first few meters above ground and this difference was even greater with 1250L90 than with 500L156 (not shown), probably due to the height of the first model level above ground. With the grid of 1250L90, the deposition impacts the first ten meters, but with the grid of 500L156, the deposition only impacts the first three meters. Less water was deposited in the second case. In the future, deposition speed ($V_{\text{deposition}}$) may be improved. In this study, $V_{\text{deposition}}$ was set to 2 cm.s^{-1}, as in the reference case of Mazoyer et al. (2017), but, as reported by Katata (2014), the deposition velocity should vary: from 2.1 cm.s^{-1} to 8.0 cm.s^{-1} over grassland and from 7.2 cm.s^{-1} to 20 cm.s^{-1} over forests. In Mazoyer et al. (2017), a sensitivity test was performed on the deposition velocity, but a larger value reduced the LWC in fog too much. In Zhang et al. (2014), however, differences were less important. Thus, deposition velocity needs to be improved to be more efficient in simulation using the 500L156 grid, taking into account turbulence or Leaf Area Index (LAI) for example. In addition, some deposition measurements realised during the SOFOG3D campaign may help to improve the deposition diagnosis in future simulations.

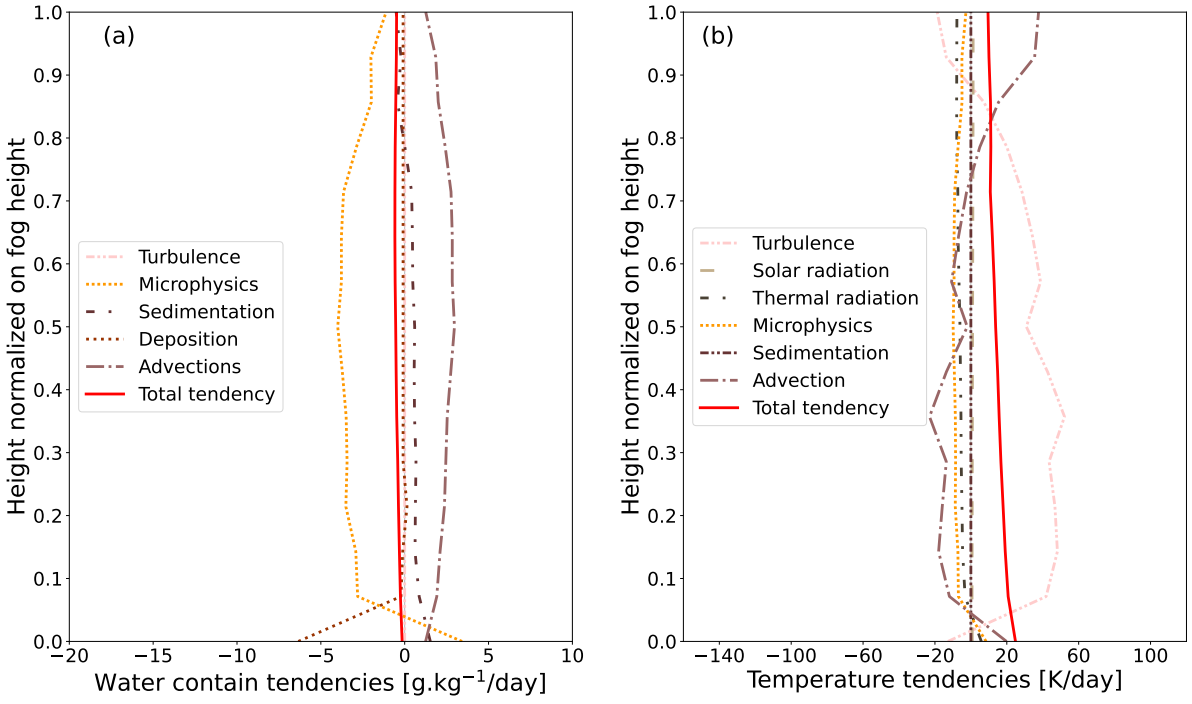

48 FIG. 9. Mean impact of processes involved in (a) water content and (b) temperature tendencies during fog
49 dissipation calculated on the dissipation subset at Agen for 500L156.

d. Dissipation delay

As for fog formation, 500L156 reduced the delay at dissipation that existed in 1250L90 (Fig. 4). In addition, 500L156 forecast thinner fogs and with less water content (Fig. 5) and forecast shorter fog events (Fig. 4).

To study these dissipation differences, the same methodology was used as for formation with the creation of a subset. Agen site was kept to create the subset and dates were conserved if: (1) fog dissipation occurred after lead time +30 in the both AROME simulations (1250L90 and 500L156) and (2) the observed fog dissipated less than 6 hours before. Subset included finally 18 fog events. For the majority of dates retained in the subset, fog forecasts by LIMA was thinner than with ICE3, water content was smaller and LIMA dissipation occurred before ICE3 dissipation.

Firstly, tests were realised on dissipation subset concerning the impact of the value of the mass closure coefficient. 1250L90 configuration was used and the forecasts with both closure

TABLE 4. Mean net SW, net LW and ground temperature tendency for the hour before fog dissipation and hour of fog dissipation, computed over the dissipation subset for the 500L156 and 500L156-ICE3 configurations.

Configuration	SW_n ($W.m^{-2}$)	LW_n ($W.m^{-2}$)	δT_{ground} ($K.h^{-1}$)
500L156	90	-45	2.05
500L156-ICE3	113	-27	2.36

coefficients, operational at 0.065 and proposed by Grant (2001) at 0.03, were compared. No differences were visible in fog dissipation, on all dates of the subset.

Processes involved in the evolution of water content in 500L156 were calculated over the hour before fog dissipation and the hour of fog dissipation over the date of the subset. They are shown in figure 9, normalized by the fog height. Water dissipation was mainly linked to microphysical processes, i.e. evaporation, and did not differ between AROME configurations (Fig. 9a). Figure 9 also shows that the temperature increased during fog dissipation and more particularly at the first level above ground. Moreover, dissipation occurred after 0600 UTC and more particularly after 0800 UTC in the subset. Dissipation may therefore be associated with sunrise.

As mentioned previously, fogs forecast with LIMA had less water content and was thinner than with ICE3. Moreover, an analysis on the dissipation subset showed that the latent heat flux required for fog dissipation was on the order of 15/30 $W.m^{-2}$ in LIMA simulations versus 50 $W.m^{-2}$ in ICE3 simulations. Thus, fogs forecast with LIMA require less energy to dissipate. Mean net Short Wave (SW_n) and net Long Wave (LW_n) fluxes and the ground temperature tendency during the last hour before fog dissipation and during the hour of fog dissipation were computed on the dissipation subset for the configurations 500L156 and 500L156-ICE3 (Tab. 4). First, SW flux was a bit greater in the simulation with LIMA, less SW was absorbed by the fog and so more SW reached the ground to heat it. The heat was then transferred to the atmosphere by LW radiation, increasing turbulence and causing fog dissipation by the bottom. LW_u radiation was greater in the simulation with LIMA in all cases, once again facilitating fog dissipation compared to simulation with ICE3. Heat transfer by turbulence on the first level is shown in figure 9b. Warming of the first level above the ground was due to advective, evaporation and thermal radiation processes. A small part of this heating was transported by vertical turbulence to the upper levels. Above the first

level, the fog layer heating was mainly linked to the vertical transport of warm air from the levels over the fog top. Over the top of the fog, the heating of air mass was due to advective process.

Fogs simulated with LIMA were thinner with less water content than those simulated using ICE3. They needed thus less energy to be dissipated. In addition, the latent heat flux flux in the last hour before fog dissipation was lower in the LIMA simulation. As a result, surface heat fluxes leading to fog dissipation were stronger in LIMA, which enables even faster fog dissipation when compared to ICE3.

7. Conclusions and outlook

In this study, observations from the SOFOG3D field campaign were used to evaluate the fog forecast quality of AROME simulations, in a reference simulation close to the operational AROME-France configuration (1250L90) and in a new configuration dedicated to fog forecasting (500L156):

- Horizontal and vertical resolutions have been improved,
- The one-moment ICE3 microphysical scheme was replaced by the 2-moment scheme LIMA, to improve the representation of droplets and the link with radiation and aerosols, and,
- the process of droplet deposition on the vegetation has been parameterized.

Evaluation of this new configuration was done along 3 axis: (1) evaluation of the quality of fog forecasts using with a statistical score study, followed by (2) an evaluation of the dynamics of the fog life cycle, to finish with (3) an evaluation of the structure and microphysical properties of the fogs. This method highlighted the specificities of the new configuration in terms of fog forecasting:

(1) A better description of the first meters above the ground, with more model levels and with thinner thicknesses, allowed a better description of turbulence in the first model levels in 500L156 forecasts. Particularly important in the early stage of fog formation, the best description of turbulence allowed the reduction of fog formation delay with the 500L156 configuration.

(2) In line with this, favouring fog formation leads to an increase in the number of fog events forecast by the new model configuration compared to the reference simulation forecasts. Increasing the number of forecast fog events increased the detection rate, but also the false alarm rate. The

increase in the number of forecast fog events should also be linked to the parameterization of the cloud scheme, identical between the two configurations.

(3) In addition, the droplet number concentration was a prognostic variable of the LIMA microphysical scheme, unlike in the ICE3 scheme where it was a constant. Thus, it allowed to forecast droplet concentrations much more realistically, although they were somewhat underestimated.

(4) Added fog events forecast by 500L156 were, however, very often short fog events (less than 4 hours), with low liquid water content (less than 20 $g.m^{-2}$) and low top height (less than 50 m). These fogs were underestimated by 1250L90. Likewise, the overestimation of thick fogs, with a fog top height upper than 100 m, and with high LWP, more than 30 $g.m^{-2}$, was reduced with the new model configuration. This improvement could be associated with the use of the 2-moment microphysical scheme LIMA, and specifically to the lower droplet concentration forecast by the model compared to the fixed value of 300 cm^{-3} used in the ICE3 microphysical scheme.

(5) These differences due to the use of the 2-moment microphysical scheme LIMA with taking into account of deposition process reduced the fog dissipation delay highlighted in the 1250L90 forecasts.

In the present statistical study and during the SOFOG3D field campaign, some biases and issues were highlighted in the model. A complementary study dedicated to case studies must be carried out. These configurations will be compared to some IOPs from the SOFOG3D field campaign. IOPs can also be used to improve the deposition parametrization (as taking into account of vegetation type Katata (2014); Mazoyer et al. (2017) or include other prognostic variables when it is possible as done in Gultepe and Milbrandt (2007)) and to test new improvements such as the use of a more realistic aerosol population to initialize LIMA free CCN field.

In France, Météo France plans to implement a NWP model using a hectometric resolution (COP 2017 - 2021, 2022 - 2026) over different areas where weather conditions may have substantial impacts. More specifically, a hectometric NWP model will be set up over Paris airports, airports which are highly impacted by fog events (Roquelaure et al. 2009). If our results are also valid for this area, the new AROME configuration, 500L156, is the best configuration that could be implemented to fog forecast. This configuration needs to be evaluated on other meteorological

situations (convection, heat waves, etc). Nevertheless, this new configuration was about 20 times more costly than reference simulation (on the same forecast domain). Operational constraints, such as numerical cost, must be taken into account and may lead to some adaptation of this configuration before its first operational implementation.

Acknowledgments. The instrumental data used in this study are parts of the SOFOG3D experiment. The SOFOG3D field campaign was supported by Météo-France and ANR through grant AAPG 2018-CE01-0004. Data are managed by the French national center for Atmospheric data and services AERIS. The authors would like to thank all those who made this work possible and all those who contributed to the writing of this article (Yves Bouteloup, François Bouyssel, Ingrid Etchevers, Christine Lac, Olivier Mestre, Matthieu Plu and the anonymous reviewers).

Data availability statement. The data are available from the authors upon request.

APPENDIX A

Scores

If a is the number of observed and forecast fog events, b is the number of unobserved but forecast fog events, c is the number of observed but not forecast fog events and d is the number of unobserved and not forecast fog events, summarized in Table A1,statistical scores are defined as follows:

TABLE A1. Contingency table.

FOG	OBSERVED: YES	OBSERVED: NO
FORECAST: YES	a	b
FORECAST: NO	c	d

$$\text{Hit Rate: } HR = \frac{a}{a+c}. \tag{A1}$$

$$\text{False Alarm Rate: } FAR = \frac{b}{a+b}. \tag{A2}$$

$$\text{Frequency Bias Index: } FBI = \frac{a+b}{a+c}. \tag{A3}$$

References

Bell, A., P. Martinet, O. Caumont, B. Vié, J. Delanoë, J.-C. Dupont, and M. Borderies, 2021: W-band radar observations for fog forecast improvement: an analysis of model and forward operator errors. *Atmospheric Measurement Techniques*, **14 (7)**, 4929 – 4946, https://doi.org/10.5194/amt-14-4929-2021.

Bengtsson, L., and Coauthors, 2017: The HARMONIE–AROME Model Configuration in the ALADIN–HIRLAM NWP System. *Monthly Weather Review*, **145 (5)**, 1919 – 1935, https://doi.org/10.1175/MWR-D-16-0417.1.

Bentzien, S., and P. Friederichs, 2012: Generating and Calibrating Probabilistic Quantitative Precipitation Forecasts from the High-Resolution NWP Model COSMO-DE. *Weather and Forecasting*, **27 (4)**, 988 – 1002, https://doi.org/10.1175/WAF-D-11-00101.1.

Bergot, T., 2013: Small-scale structure of radiation fog: a large-eddy simulation study. *Quarterly Journal of the Royal Meteorological Society*, **139 (673)**, 1099 – 1112, https://doi.org/10.1002/qj.2051.

Bergot, T., J. Escobar, and V. Masson, 2015: Effect of small-scale surface heterogeneities and buildings on radiation fog: Large-eddy simulation study at Paris–Charles de Gaulle airport. *Quarterly Journal of the Royal Meteorological Society*, **141 (686)**, 285 – 298, https://doi.org/10.1002/qj.2358.

Bergot, T., and D. Koracin, 2021: Observation, Simulation and Predictability of Fog: Review and Perspectives. *Atmosphere*, **12 (2)**, https://doi.org/10.3390/atmos12020235.

Bergot, T., and R. Lestringant, 2019: On the Predictability of Radiation Fog Formation in a Mesoscale Model: A Case Study in Heterogeneous Terrain. *Atmosphere*, **10 (4)**, 165, https://doi.org/10.3390/atmos10040165.

Boutle, I., J. Price, I. Kudzotsa, H. Kokkola, and S. Romakkaniemi, 2018: Aerosol–fog interaction and the transition to well-mixed radiation fog. *Atmospheric Chemistry and Physics*, **18 (11)**, 7827 – 7840, https://doi.org/10.5194/acp-18-7827-2018.

Boutle, I., and Coauthors, 2022: Demistify: a large-eddy simulation (LES) and single-column model (SCM) intercomparison of radiation fog. *Atmospheric Chemistry and Physics*, **22 (1)**, 319 – 333, https://doi.org/10.5194/acp-22-319-2022.

Boutle, I. A., A. Finnenkoetter, A. P. Lock, and H. Wells, 2016: The London Model: forecasting fog at 333 m resolution. *Quarterly Journal of the Royal Meteorological Society*, **142 (694)**, 360 – 371, https://doi.org/10.1002/qj.2656.

Brousseau, P., Y. Seity, D. Ricard, and J. Léger, 2016: Improvement of the forecast of convective activity from the AROME-France system. *Quarterly Journal of the Royal Meteorological Society*, **142 (699)**, 2231–2243, https://doi.org/10.1002/qj.2822.

Burnet, F., and Coauthors, 2020: The SOuth west FOGs 3D experiment for processes study (SoFog3D) project. *EGU General Assembly Conference Abstracts*, 17836, https://doi.org/10.5194/egusphere-egu2020-17836.

Canut, G., F. Couvreux, M. Lothon, D. Legain, B. Piguet, A. Lampert, W. Maurel, and E. Moulin, 2016: Turbulence fluxes and variances measured with a sonic anemometer mounted on a tethered balloon. *Atmospheric Measurement Techniques*, **9 (9)**, 4375 – 4386, https://doi.org/10.5194/amt-9-4375-2016.

COP, 2017 - 2021: Contrat d'objectifs et de performance de Météo-France - 2017-2021. *Météo-France communication*, URL https://meteofrance.fr/sites/meteofrance.fr/files/files/editorial/COP_2017_2021_VF.pdf.

COP, 2022 - 2026: Contrat d'objectifs et de performance de Météo-France - 2022-2026. *Météo-France communication*, URL https://meteofrance.fr/sites/meteofrance.fr/files/files/editorial/Rapport_COP_V14.pdf.

de Rooy, W. C., and Coauthors, 2022: Model development in practice: a comprehensive update to the boundary layer schemes in HARMONIE-AROME cycle 40. *Geoscientific Model Development*, **15 (4)**, 1513 – 1543, https://doi.org/10.5194/gmd-15-1513-2022.

Delanoë, J., and Coauthors, 2016: BASTA: A 95-GHz FMCW Doppler radar for cloud and fog studies. *Journal of Atmospheric and Oceanic Technology*, **33 (5)**, 1023 – 1038, https://doi.org/10.1175/JTECH-D-15-0104.1.

Ducongé, L., C. Lac, B. Vié, T. Bergot, and J. D. Price, 2020: Fog in heterogeneous environments: the relative importance of local and non-local processes on radiative-advective fog formation. *Quarterly Journal of the Royal Meteorological Society*, **146 (731)**, 2522 – 2546, https://doi.org/10.1002/qj.3783.

Dupont, J.-C., M. Haeffelin, A. Protat, D. Bouniol, N. Boyouk, and Y. Morille, 2012: Stratus–Fog Formation and Dissipation: A 6-Day Case Study. *Boundary-Layer Meteorology*, **143**, 207 – 225, https://doi.org/10.1007/s10546-012-9699-4.

Fathalli, M., C. Lac, F. Burnet, and B. Vié, 2022: Formation of fog due to stratus lowering: An observational and modelling case study. *Quarterly Journal of the Royal Meteorological Society*, **148 (746)**, 2299 – 2324, https://doi.org/https://doi.org/10.1002/qj.4304.

Fernando, H. J. S., and Coauthors, 2021: C-FOG: Life of Coastal Fog. *Bulletin of the American Meteorological Society*, **102 (2)**, 244 – 272, https://doi.org/10.1175/BAMS-D-19-0070.1.

Gadher, D., and T. Baird, 2006: Airport dash as the fog lifts. *The Sunday Times*, URL https://www.thetimes.co.uk/article/airport-dash-as-the-fog-lifts-jtx5j5hxrnz.

Grant, A. L. M., 2001: Cloud-base fluxes in the cumulus-capped boundary layer. *Quarterly Journal of the Royal Meteorological Society*, **127 (572)**, 407 – 421, https://doi.org/10.1002/qj.49712757209.

Gultepe, I., and G. A. Isaac, 2004: Aircraft observations of cloud droplet number concentration: Implications for climate studies. *Quarterly Journal of the Royal Meteorological Society*, **130 (602)**, 2377 – 2390, https://doi.org/10.1256/qj.03.120.

Gultepe, I., and J. Milbrandt, 2007: Microphysical observations and mesoscale model simulation of a warm fog case during FRAM project. *Pure and Applied Geophysics*, **164**, 1161 – 1178, https://doi.org/10.1007.

Gultepe, I., M. D. Müller, and Z. Boybeyi, 2006: A New Visibility Parameterization for Warm-Fog Applications in Numerical Weather Prediction Models. *Journal of Applied Meteorology and Climatology*, **45 (11)**, 1469 – 1480, https://doi.org/10.1175/JAM2423.1.

Gultepe, I., M. Pagowski, and J. Reid, 2007a: A Satellite-Based Fog Detection Scheme Using Screen Air Temperature. *Weather and Forecasting*, **22 (3)**, 444 – 456, https://doi.org/10.1175/WAF1011.1.

Gultepe, I., and Coauthors, 2007b: The fog remote sensing and modeling (FRAM) field project and preliminary results. *AMS 12th Cloud Physics Conference*, 9 – 14.

Gultepe, I., and Coauthors, 2009: The Fog Remote Sensing and Modeling Field Project. *Bulletin of the American Meteorological Society*, **90 (3)**, 341 – 360, https://doi.org/10.1175/2008BAMS2354.1.

Gultepe, I., and Coauthors, 2019: A Review of High Impact Weather for Aviation Meteorology. *Pure and Applied Geophysics*, **176**, 1869 – 1921, https://doi.org/10.1007/s00024-019-02168-6.

Gultepe, I., and Coauthors, 2021: A Review of Coastal Fog Microphysics During C-FOG. *Boundary-Layer Meteorology*, **181**, 227 – 265, https://doi.org/10.1007/s10546-021-00659-5.

Katata, G., 2014: Fogwater deposition modeling for terrestrial ecosystems: A review of developments and measurements. *Journal of Geophysical Research: Atmospheres*, **119 (13)**, 8137 – 8159, https://doi.org/10.1002/2014JD021669.

Kunkel, B. A., 1984: Parameterization of Droplet Terminal Velocity and Extinction Coefficient in Fog Models. *Journal of Climate and Applied Meteorology*, **23 (1)**, 34 – 41, https://doi.org/10.1175/1520-0450(1984)023⟨0034:PODTVA⟩2.0.CO;2.

Lac, C., and Coauthors, 2018: Overview of the Meso-NH model version 5.4 and its applications. *Geoscientific Model Development*, **11**, 1929 – 1969, https://doi.org/10.5194/gmd-11-1929-2018.

Lafore, J. P., and Coauthors, 1998: The Meso-NH atmospheric simulation system. Part I: Adiabatic formulation and control simulations. *Annales Geophysicae*, **16 (1)**, 90 – 109, https://doi.org/10.1007/s00585-997-0090-6.

Long, Q., B. Wu, X. Mi, S. Liu, X. Fei, and T. Ju, 2021: Review on Parameterization Schemes of Visibility in Fog and Brief Discussion of Applications Performance. *Atmosphere*, **12 (12)**, https://doi.org/10.3390/atmos12121666.

Martin, G. M., D. W. Johnson, and A. Spice, 1994: The Measurement and Parameterization of Effective Radius of Droplets in Warm Stratocumulus Clouds. *Journal of Atmospheric Sciences*, **51 (13)**, 1823 – 1842, https://doi.org/10.1175/1520-0469(1994)051⟨1823:TMAPOE⟩2.0.CO;2.

Martinet, P., and Coauthors, 2022: A dataset of temperature, humidity, and liquid water path retrievals from a network of ground-based microwave radiometers dedicated to fog investigatio. *Bulletin of Atmospheric Science and Technology*, **3**, 6, https://doi.org/10.1007/s42865-022-00049-w.

Mathew, S., H. Llawani, S. Sawhney, and C. Walia, 2016: Airline Accidents and Airline Legislations: A Case Study Approach. *The 3rd International Aviation Management Conference*, 126 – 136.

Mazoyer, M., F. Burnet, and C. Denjean, 2022: Experimental study on the evolution of droplet size distribution during the fog life cycle. *Atmospheric Chemistry and Physics*, **22 (17)**, 11 305–11 321, https://doi.org/10.5194/acp-22-11305-2022.

Mazoyer, M., C. Lac, O. Thouron, T. Bergot, V. Masson, and L. Musson-Genon, 2017: Large eddy simulation of radiation fog: impact of dynamics on the fog life cycle. *Atmospheric Chemistry and Physics*, **17 (21)**, 13 017 – 13 035, https://doi.org/10.5194/acp-17-13017-2017.

Milmo, D., 2007: BAA count the cost of December fog. *The Guardian*, URL https://www.theguardian.com/business/2007/jan/09/theairlineindustry.travel.

Pagowski, M., I. Gultepe, and P. King, 2004: Analysis and Modeling of an Extremely Dense Fog Event in Southern Ontario. *Journal of Applied Meteorology*, **43 (1)**, 3 – 16, https://doi.org/10.1175/1520-0450(2004)043⟨0003:AAMOAE⟩2.0.CO;2.

Pergaud, J., V. Masson, S. Malardel, and F. Couvreux, 2009: A Parameterization of Dry Thermals and Shallow Cumuli for Mesoscale Numerical Weather Prediction. *Boundary-Layer Meteorology*, **132**, 83 – 106, https://doi.org/10.1007/s10546-009-9388-0.

Pezzoli, A., M. Moncalero, A. Boscolo, E. Cristofori, F. Giacometto, S. Gastaldi, and G. Vercelli, 2010: The meteohydrological analysis and the sport performance: which are the connections? The case of the XXI Winter Olympic Games, Vancouver 2010. *The Journal of sports medicine and physical fitness*, **50**, 19 – 20.

Philip, A., 2016: Apport d'une résolution verticale plus fine dans le calcul des tendances physiques pour la modélisation du brouillard dans le modèle AROME. Ph.D. thesis, Université de Toulouse 3 Paul Sabatier, URL http://www.theses.fr/2016TOU30261/document, thèse de doctorat dirigée par Bergot Thierry, Bouteloup Yves et Bouyssel François.

Philip, A., T. Bergot, Y. Bouteloup, and F. Bouyssel, 2016: The impact of Vertical resolution on fog forecasting in the kilometric-scale model AROME: a case study and statistics. *Weather and Forecasting*, **31 (5)**, 1655 – 1671, https://doi.org/10.1175/WAF-D-16-0074.1.

Pinty, J., and P. Jabouille, 1998: A mixed-phase cloud parameterization for use in a mesoscale non-hydrostatic model: simulations of a squall line and of orographic precipitations. *Conf. on Cloud Physics*, American Meteorology Society Everett, WA, 217 – 220.

Price, J. D., and R. Clark, 2014: On the Measurement of Dewfall and Fog-Droplet Deposition. *Boundary-Layer Meteorology*, **152**, https://doi.org/10.1007/s10546-014-9930-6.

Price, J. D., and Coauthors, 2018: LANFEX: A Field and Modeling Study to Improve Our Understanding and Forecasting of Radiation Fog. *Bulletin of the American Meteorological Society*, **99 (10)**, 2061 – 2077, https://doi.org/10.1175/BAMS-D-16-0299.1.

Román-Cascón, C., C. Yagüe, G.-J. Steeneveld, G. Morales, J. A. Arrillaga, M. Sastre, and G. Maqueda, 2019: Radiation and cloud-base lowering fog events: Observational analysis and evaluation of WRF and HARMONIE. *Atmospheric Research*, **229**, 190 – 207, https://doi.org/10.1016/j.atmosres.2019.06.018.

Rooy, W. D., C. D. Bruijn, S. Tijm, R. Neggers, P. Siebesma, , and J. Barkmeijer, 2010: Experiences with Harmonie at KNMI. *HIRLAM Newsletter*, **56**, 21 – 29.

Roquelaure, S., R. Tardif, S. Remy, and T. Bergot, 2009: Skill of a Ceiling and Visibility Local Ensemble Prediction System (LEPS) according to Fog-Type Prediction at Paris-Charles de Gaulle Airport. *Weather and Forecasting*, **24 (6)**, 1511 – 1523, https://doi.org/10.1175/2009WAF2222213.1.

Ryznar, E., 1977: Advection-radiation fog near lake Michigan. *Atmospheric Environment (1967)*, **11 (5)**, 427 – 430, https://doi.org/10.1016/0004-6981(77)90004-X.

Seity, Y., P. Brousseau, S. Malardel, G. Hello, P. Bénard, F. Bouttier, C. Lac, and V. Masson, 2011: The AROME-France Convective-Scale Operational Model. *Monthly Weather Review*, **139 (3)**, 976–991, https://doi.org/10.1175/2010MWR3425.1.

Spiegel, J. K., P. Zieger, N. Bukowiecki, E. Hammer, E. Weingartner, and W. Eugster, 2012: Evaluating the capabilities and uncertainties of droplet measurements for the fog droplet spectrometer (FM-100). *Atmospheric Measurement Techniques*, **5 (9)**, 2237 – 2260, https://doi.org/10.5194/amt-5-2237-2012.

Steeneveld, G.-J., and M. de Bode, 2018: Unravelling the relative roles of physical processes in modelling the life cycle of a warm radiation fog. *Quarterly Journal of the Royal Meteorological Society*, **144 (714)**, 1539 – 1554, https://doi.org/https://doi.org/10.1002/qj.3300.

Stolaki, S., M. Haeffelin, C. Lac, J.-C. Dupont, T. Elias, and V. Masson, 2015: Influence of aerosols on the life cycle of a radiation fog event. A numerical and observational study. *Atmospheric Research*, **151**, 146 – 161, https://doi.org/10.1016/j.atmosres.2014.04.013.

Tardif, R., 2007: The Impact of Vertical Resolution in the Explicit Numerical Forecasting of Radiation Fog: A Case Study. *Pure and Applied Geophysics*, **164**, 1221 – 1240, https://doi.org/10.1007/s00024-007-0216-5.

Tardif, R., and R. M. Rasmussen, 2007: Event-Based Climatology and Typology of Fog in the New York City Region. *Journal of Applied Meteorology and Climatology*, **46 (8)**, 1141–1168, https://doi.org/10.1175/JAM2516.1.

Vié, B., J.-P. Pinty, S. Berthet, and M. Leriche, 2016: LIMA (v1.0): A quasi two-moment microphysical scheme driven by a multimodal population of cloud condensation and ice freezing nuclei. *Geoscientific Model Development*, **9 (2)**, 567 – 586, https://doi.org/10.5194/gmd-9-567-2016.

von Glasow, R., and A. Bott, 1999: Interaction of radiation fog with tall vegetation. *Atmospheric Environment*, **33 (9)**, 1333 – 1346, https://doi.org/10.1016/S1352-2310(98)00372-0.

Westerhuis, S., O. Fuhrer, J. Cermak, and W. Eugster, 2020: Identifying the key challenges for fog and low stratus forecasting in complex terrain. *Quarterly Journal of the Royal Meteorological Society*, **146 (732)**, 3347 – 3367, https://doi.org/10.1002/qj.3849.

World Meteorological Organisation, W. M. O., 2017: Fog. *International Cloud Atlas*, URL https://cloudatlas.wmo.int/en/fog.html.

Zhang, X., L. Musson-Genon, E. Dupont, M. Milliez, and B. Carissimo, 2014: On the influence of a simple microphysics parametrization on radiation fog modelling: A case study during parisfog. *Boundary-layer meteorology*, **151 (2)**, 293 – 315, https://doi.org/10.1007/s10546-013-9894-y.